第 50 卷 第 1 期/2023 年 1 月/中国激光 特邀论文

中国激光

银纳米线-三角片耦合结构发射光的偏振依赖特性

李圆圆，杨龙坤，李志鹏*

首都师范大学物理系纳米光子与纳米材料北京市重点实验室，北京 100048

摘要 银纳米线可以承载传播的表面等离激元，纳米片可以产生局域的表面等离激元，二者形成的耦合结构不但可以将传播光场耦合为局域增强光场，还可以调控光场的偏振态等性质，为纳米光调控提供新的自由度。本团队构建了银纳米线-三角片耦合结构，并发现耦合结构的发射偏振与纳米线-三角片的耦合方式有关：当三角片与纳米线之间是“线”接触耦合时，耦合结构的发射偏振随着激发偏振的旋转而旋转；当二者是“点”接触耦合时，无论激发偏振如何变化，发射偏振角度几乎保持160°不变。进一步，利用时域有限差分法验证了出射偏振对入射偏振的依赖特性。通过计算自由电流密度体积分揭示了纳米线中传播的表面等离激元模式与银纳米线-三角片耦合模式的转化机制，以及不同表面等离激元模式的叠加对发射偏振的调控。这些发现为纳米尺度上的光调控以及在纳米尺度上构建纳米光子器件提供了更多灵活性。

关键词 光学材料；表面等离激元；纳米结构；发射；偏振依赖性

中图分类号 O436 **文献标志码** A **DOI**：10.3788/CJL221291

1 引 言

20世纪50年代，表面等离激元(SPPs)引起了众多科学家的广泛关注[1]。表面等离激元可将光场束缚在金属纳米结构周围，从而突破光的衍射极限[2]，实现光学器件的微型化和高度集成化。用光子代替电子作为信息载体，为构建大带宽、高速度和低耗散的集成纳米光子器件提供了更具前景的平台[3]。目前，各种基于表面等离激元的微纳光学元件被开发出来，如波导[4-7]、谐振器[8]、纳米天线[9-12]、多路复用器[13]和光开关[14]等。一些研究者利用金属纳米结构的等离子体共振特性实现了在纳米尺度上对光的操控[15]，其中，对光的偏振态进行调控在集成芯片、传感器[16-20]和量子通信[21]等领域具有重要意义。

化学合成的金属纳米结构，如银纳米线，具有表面光滑、产率高、传输损耗低等优势，可以实现纳米尺度的光场传导，为构建功能化的集成光子回路奠定了基础。已有研究表明，可以对银纳米线中传播的表面等离激元的发射进行调控[22]。此外，研究人员在纳米线和纳米颗粒耦合体系光学性质的调控方面取得了一些成果，例如：银纳米线附近的纳米颗粒可作为光学天线，促进光的有效耦合[23]；纳米线与纳米颗粒耦合处的近场增强和远场发射可以通过改变入射偏振进行调制[24-28]，从而构建具有偏振依赖性的路由器/分束器[29-33]、调制器[34-36]和逻辑门[37-39]等器件。因此，通过组装不同的耦合体系可以为实现纳米光子器件的偏振调控提供更多自由度。

本文主要研究了银纳米线-三角片耦合结构的出射偏振和入射偏振之间的依赖关系。结果显示，三角片与纳米线之间的耦合方式对偏振依赖性调控起着非常关键的作用：当三角片与纳米线为“线”接触耦合时，发射光的偏振随着激发偏振的增大而单调增大；当两者呈“点”接触时，无论激发偏振如何变化，发射偏振几乎保持160°不变。理论上，可以通过纳米线中传播表面等离激元模式与纳米线-三角片耦合模式的转换、叠加来理解体系的发射机制。本文研究结果为纳米尺度上的光偏振操纵提供了新的可能性，并进一步推动了集成纳米光子器件的发展。

2 实验原理与方法

2.1 样品的制备

化学合成的银纳米线的长度约为5～20 μm，平均直径为300 nm。银纳米颗粒的大小不同，形状各异，有立方块、三角片、棒状和球形等。制备步骤如下：

1）将700 mg聚乙烯吡咯烷酮(PVP，相对分子质量MW为30000)、1000 mg硝酸银和少量氯化钠依次放入10 mL乙二醇(EG)溶液中，进行连续磁力搅拌，使之充分溶解；

2）将混合溶液置于160 ℃的环境下加热90 min；

收稿日期：2022-10-05；**修回日期**：2022-11-06；**录用日期**：2022-11-09

基金项目：国家重点研发计划(2021YFA1400800)、北京市自然科学基金(Z190006)、国家青年人才支持计划、国家自然科学基金(11704266，11774245)

通信作者：*zhipeng-jlu@163.com

3）待混合溶液冷却至室温后，用丙酮和乙醇将制备的纳米线和纳米颗粒混合物进行离心处理，除去其中的EG和PVP；

4）收集沉淀物，并用乙醇分散，以备后续使用；

5）将混合物的悬浮液滴到铟锡氧化物（ITO）覆盖的玻璃基底上，在室温条件下自然风干，自组装形成纳米线-三角片耦合结构。

由于在接下来的实验中需要对不同的耦合体系精确定位，因此需要进行扫描电子显微镜（SEM）测量。

2.2　实验系统与原理

为了防止样品在空气中氧化或硫化，用SEM表征后，及时滴上折射率n=1.518的显微镜油进行光学测量。具体的实验装置如图1所示。波长为633 nm的He-Ne激光通过100×油镜（Olympus UPlanFLN，数值孔径NA=1.3）聚焦在银纳米线的一端，激光偏振可以通过旋转半波片来改变。从纳米线-三角片耦合处发出的光用同一物镜收集，进而被安装在倒置光学显微镜（OLYMPUS IX71S1F-3）上的电荷耦合器件（CCD）探测。为了得到出射光的偏振，在CCD前添加了一块偏振片。

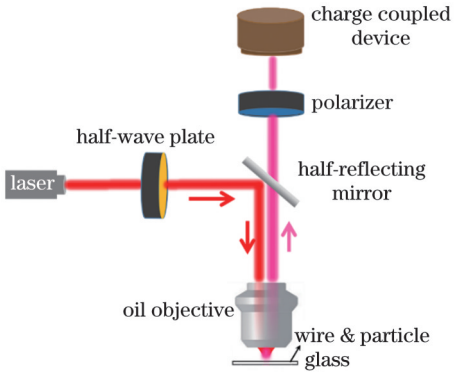

图1　实验装置示意图

Fig. 1　Scheme of experimental setup

3　分析与讨论

3.1　实验结果

如图2（a）中的SEM图所示，长为12.4 μm、直径为389 nm的银纳米线与边长为556 nm的三角片耦合，插图是银纳米线和三角片耦合处的局部放大图。通过物镜将激光聚焦到纳米线端头，激发纳米线中传

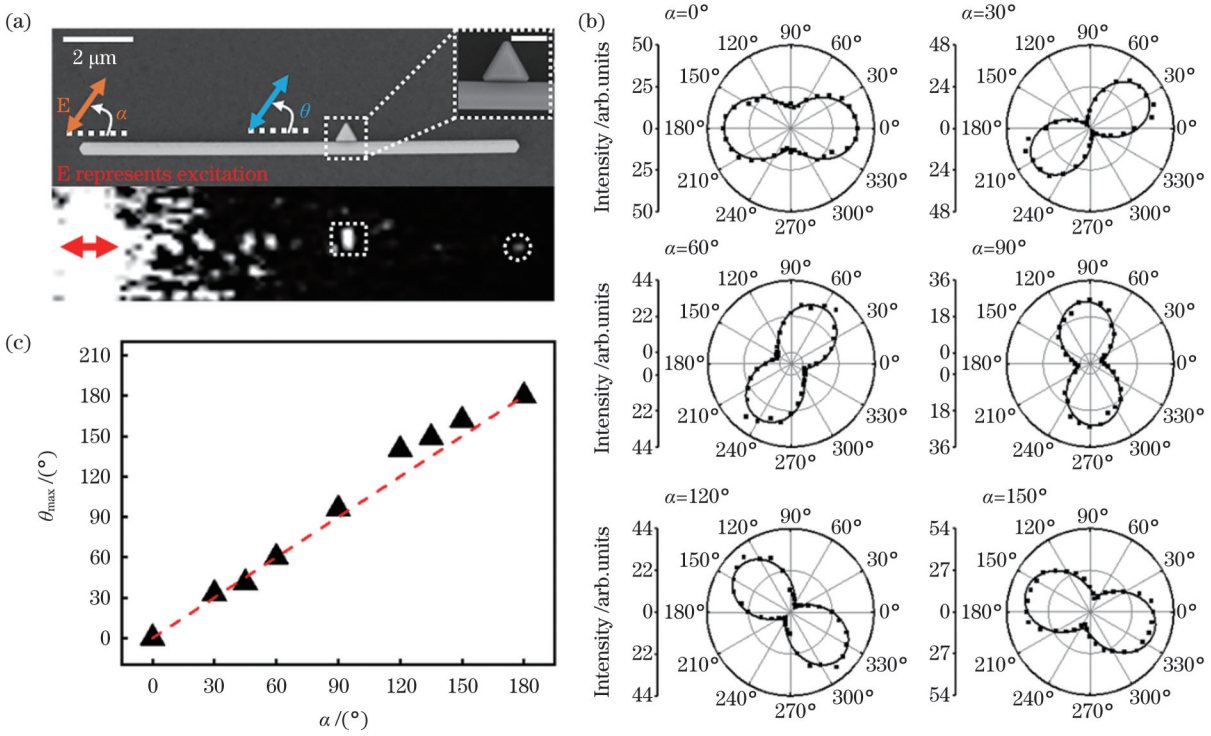

图2　银纳米线-三角片耦合结构的发射偏振特性。（a）耦合结构的SEM图，上方插图是三角片与纳米线耦合处的局部放大图（标尺为500 nm），下图是633 nm激光激发纳米线时的光学成像图（红色箭头表示激光的偏振）；（b）入射偏振角度α为0°、30°、60°、90°、120°和150°时，发射强度随偏振片旋转角度θ的变化（黑色曲线是拟合结果，入射偏振和偏振片相对纳米线轴逆时针旋转）；（c）发射偏振角度θ_{max}与激发偏振角度α之间的关系

Fig. 2　Emission polarization at silver nanowire-triangular plate coupled structure. (a) SEM images of nanowire-triangular plate coupled structure, where the upper inset is a partially magnified view of coupled junction between triangular plate and nanowire (scale bar is 500 nm) and the corresponding optical image of the nanowire under excitation of a 633 nm laser spot is shown in the bottom (the red arrow indicates the polarization of the laser); (b) emission intensity as a function of polarizer rotation angle θ at incident polarization degree α=0°, 30°, 60°, 90°, 120° and 150°, respectively (black curves are fitting results, the incident polarization and polarizer rotate anticlockwise relative to nanowire axis); (c) correlation between emission polarization angle θ_{max} and excitation polarization angle α

播的表面等离激元，表面等离激元最终在三角片和纳米线末端通过散射以光子的形式辐射到自由空间。在图 2(a)所示的光学成像中，耦合处(虚线框)和纳米线末端(虚线圈)的亮点即为表面等离激元出射的光斑。已有工作发现表面等离激元传播到纳米线末端后会以一定的角度重新发射到自由空间，且偏振特性与端头形貌有关[22,40]。然而，纳米线与三角片耦合处的发射与纳米线端头的散射不同，其光斑更明显[如图 2(a)中的虚线框所示]，表明此处的等离激元与光子间的转换效率更高[23-24]。因此，本文进一步探究了纳米线与三角片耦合处的发射偏振及其与激发偏振的依赖关系。测量了纳米线与三角片耦合处发射光的强度随偏振片旋转角度 θ 的变化，结果如图 2(b)所示。当激发偏振平行于纳米线时，发射光的偏振也平行于纳米线。在此，本文将发射偏振角度定义为最大发射强度对应的偏振片旋转角度 θ_{max}。由于杂散光仅会影响耦合处发射光强度最小值的测量，所以杂散光对发射偏振测量的影响较小。如图 2(c)所示，随着入射(激发)偏振角度 α 增大，发射偏振角度 θ_{max} 增大。

另外，对其他纳米线-三角片耦合体系也进行了测量。如图 3(a)所示，三角片与长为 6.7 μm、直径为 253 nm 的纳米线为“点”接触耦合。激光激发纳米线端头后，耦合处同样出现了明亮的发射光斑。通过旋转半波片和偏振片测量了不同激发偏振下耦合处发射光强度随偏振片旋转角度的变化，测量结果如图 3(b)所示。可以发现，发射光的偏振与激发偏振无关，几乎保持 160°不变，如图 3(c)所示。虽然图 2 和图 3 中展示的耦合系统均是由纳米线与三角片组成的，但它们的发射偏振特性却完全不同，这些特性为构建功能化等离激元器件提供了更多自由度。

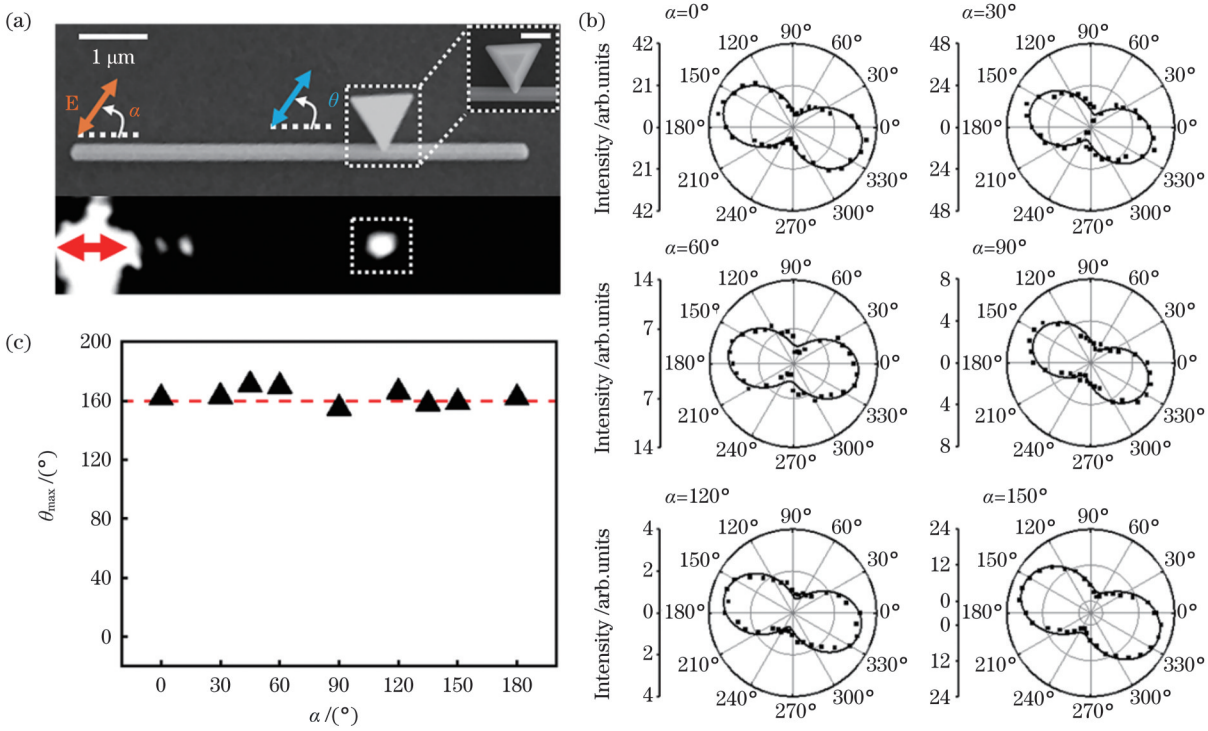

图 3 其他银纳米线-三角片耦合结构的发射偏振测量。(a)耦合体系的 SEM 图，上方插图是三角片与纳米线耦合处的局部放大图(标尺为 500 nm)，下图是激光激发纳米线左端后的光学图像；(b)耦合处的发射强度随偏振片旋转角度 θ 的变化；(c)发射偏振角度 θ_{max} 和激发偏振角度 α 之间的关系

Fig. 3 Emission polarization measurement of another nanowire-triangular plate coupled structure. (a) SEM images of coupled structure, where the upper inset is an enlarged image of coupled junction between triangular plate and nanowire (the scale bar is 500 nm) and the corresponding optical image of the left end of nanowire under laser excitation is shown in the bottom; (b) emission intensity at the junction as a function of polarizer rotation angle θ; (c) correlation between emission polarization angle θ_{max} and excitation polarization angle α

3.2 理论模拟

为了理解纳米线-三角片耦合体系的不同发射特性，利用时域有限差分(FDTD)法进行了模拟。图 4(a)是纳米线与三角片耦合示意图。用高斯光束(λ=633 nm)激发纳米线一端，得到三角片与纳米线耦合的局域近场分布，然后将其投影到半径为 1 m 的远场球面上，对收集范围内的辐射场进行积分(收集角度为 60°)，计算发射场偏振。通过改变三角片与纳米线的耦合方式，研究了体系的发射偏振与激发偏振之间的依赖关系。如图 4(b)所示，当三角片与纳米线是“线”接触耦合时，表面等离激元会在间隙中传播，形成法布里-珀罗共振腔。此时，发射偏振角度 θ_{max} 随着激发偏振角度 α 的增大而增大，这与图 2 所示的实验结果相对应。然而，当两者为“点”接触耦合时，电场主要分布在三角片上，如图 4(c)所示。可以

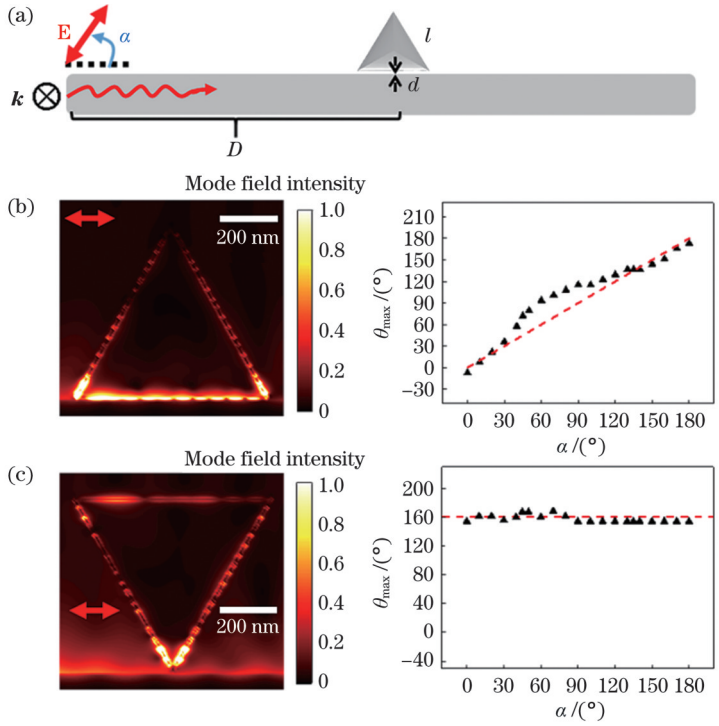

图 4 模拟得到的不同纳米线-三角片耦合体系的发射偏振。(a)耦合结构的示意图，长为 5 μm、直径为 300 nm 的纳米线和边长 l=686 nm 的三角片均处在介电常数 ε=1.5 的均匀介电环境中，用高斯光束(λ=633 nm)激发纳米线(d=10 nm，D=3.3 μm)左端；(b)纳米线与三角片呈“线”接触耦合的近场分布图(左图)以及相应的远场发射偏振与激发偏振的依赖关系(右图)，其中红色箭头表示平行的入射偏振(α=0°)；(c) 纳米线与三角片呈“点”接触耦合的近场分布图(左图)以及相应的远场发射偏振与激发偏振的依赖关系(右图)

Fig. 4 Calculated emission polarization of different nanowire-triangular plate coupled structures. (a) Schematic of coupled structure, where the nanowire with length of 5 μm and diameter of 300 nm and triangular plate with side length l=686 nm are located in a homogeneous dielectric background with dielectric constant ε=1.5, and the left end of the nanowire (d=10 nm, D=3.3 μm) is excited by a 633 nm Gaussian beam; (b) near-field distribution of nanowire-triangular plate with “line” coupling type (left figure) and corresponding dependence between far-field emission polarization and excitation polarization (right figure), where the red arrow indicates the parallel incident polarization (α=0°); (c) near-field distribution of nanowire-triangular plate with “point” coupling type (left figure) and corresponding dependence between far-field emission polarization and excitation polarization (right figure)

发现，无论激发偏振角度如何变化，发射偏振角度几乎保持 160°不变($\theta_{max}\approx160°$)，与图 3 所示数据一致。这些结果表明三角片与纳米线耦合体系的发射偏振依赖性与两者的耦合方式密切相关。

3.3 模型讨论

以上的实验和模拟结果均说明不同纳米线-三角片耦合结构的发射偏振依赖性各不相同。为了进一步理解调节机制，本文对耦合处激发的等离激元模式进行了分析。对于单根纳米线来说，平行的入射偏振可激发 m=0 和 m=−1 两种基本的表面等离激元模式；而偏振垂直于纳米线时，m=1 和 m=2 两种模式就会被激发[41]。但在纳米线-三角片耦合体系中，只有 m=0 和 m=1 两个模式能与三角片有效耦合，从而产生纳米线-三角片耦合模式。因此，三角片与纳米线耦合处的等离激元模式主要包括杂化的纳米线模式(m=0 和 m=1)以及纳米线-三角片耦合模式 P，如图 5(a)所示。根据天线辐射理论，自由电流密度为 J 的天线发射场[42]可以表示为

$$\boldsymbol{E}=\frac{\exp(\mathrm{i}kR)}{4\pi\varepsilon_0 c^2 R}(\ddot{\boldsymbol{p}}\times\boldsymbol{e}_R)\times\boldsymbol{e}_R, \tag{1}$$

式中：$\ddot{\boldsymbol{p}}=\dfrac{\mathrm{d}\left[\int_V J(x')\mathrm{d}V'\right]}{\mathrm{d}t}$ 是电荷系统电偶极矩 $\boldsymbol{p}$ 的二阶导数，其中 x' 是电荷分布的坐标，V 是电荷分布区域的体积；k 为波矢；R 为远场球面半径；ε_0 是真空介电常数；c 为真空中光的传播速度；$\boldsymbol{e}_R$ 是径向的单位矢量。图 5(b)展示了纳米线和三角片“点”接触耦合时的局域电场分布。计算蓝色和红色区域内自由电流密度 J 的体积分，利用式(1)分别得到三角片和纳米线两部分的发射光偏振。图 5(c)显示了平行(左图)和垂直(右图)偏振激发下三角片(纳米线-三角片耦合模式 P)的发射偏振，可以发现：无论是在平行偏振激发下还是在垂直偏振激发下，三角片中等离激元模式的发射偏振均约为 160°。纳米线的发射偏振如图 5(d)所示。对于平行偏振光激发的 m=0 模式，其对应的电荷沿着纳米线方向振荡，导致纳米线产生的发射光的偏振方向与纳米线轴线平行；对于垂直偏振光激发的 m=1 模式，其发射偏振为 90°[22]。另外，三角片与纳米线呈“线”接触时，纳米线中的等离激元模式耦合到间隙中传播形成法布里-珀罗腔，此时主要是纳米线的等离激元模式占主导。如图 6

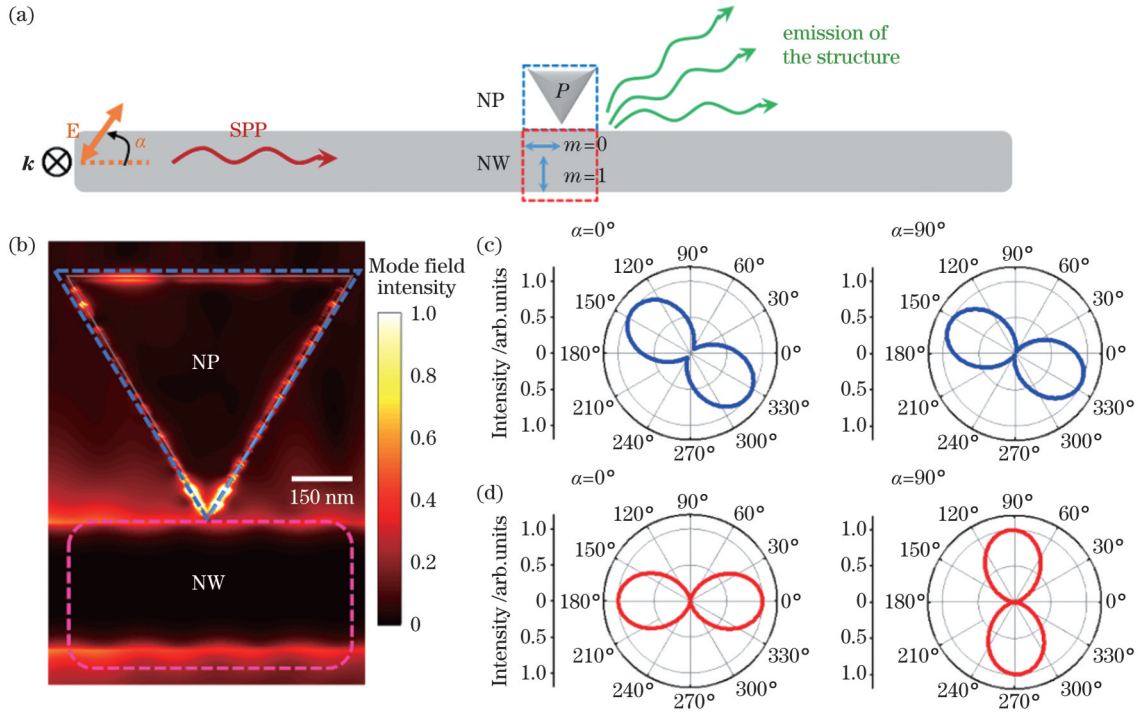

图 5 计算得到的纳米线(NW)和三角片(NP)的发射偏振。(a)银纳米线与三角片“点”耦合示意图;(b)纳米线与三角片耦合处的局域电场分布;(c)平行和垂直激发偏振下三角片(蓝色)的发射偏振角度分别是 144°和 156°;(d)平行和垂直激发偏振下纳米线(红色)的发射偏振角度分别为 0°和 90°

Fig. 5 Calculated emission polarization of nanowire (NW) and triangular plate (NP). (a) Schematic of Ag nanowire and triangular plate “point” coupling; (b) localized electric field distribution of nanowire and triangular plate coupled junction; (c) emission polarization angle of triangular plate (blue) is 144° and 156° under the parallel and perpendicular excitation polarization, respectively; (d) emission polarization angle of nanowire (red) is 0° and 90° under the parallel and perpendicular excitation polarization, respectively

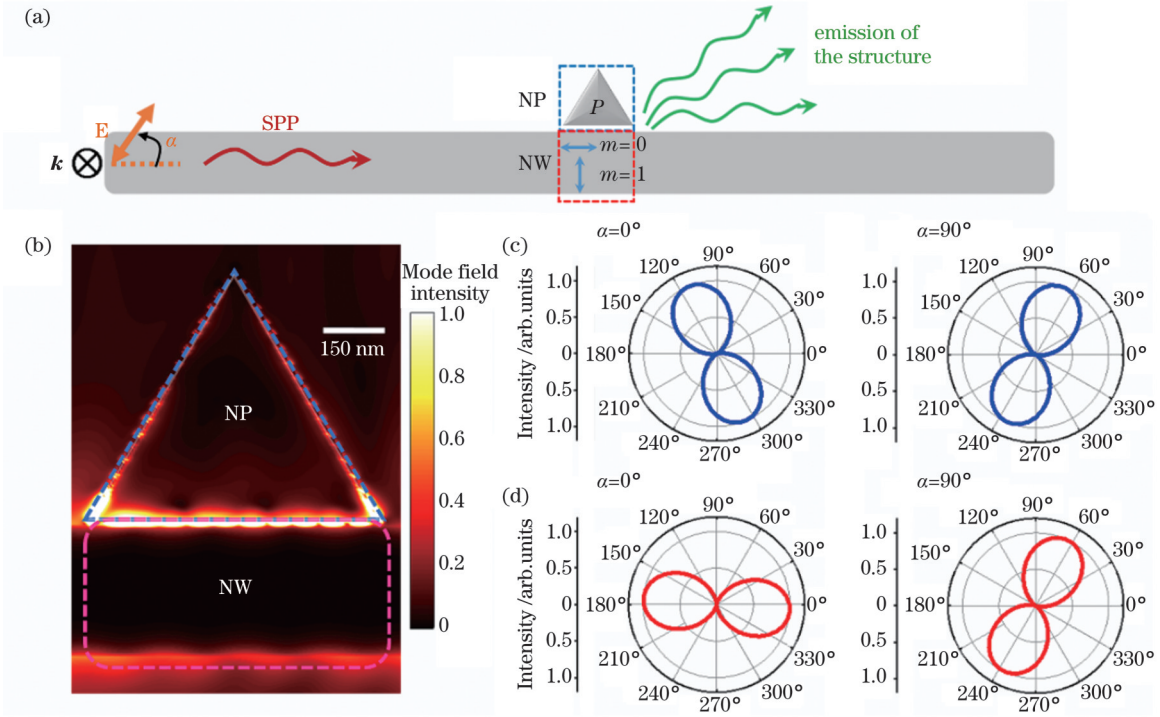

图 6 计算得到的纳米线和三角片的发射偏振。(a)银纳米线-三角片“线”耦合示意图;(b)局域电场分布;(c)平行和垂直激发偏振下三角片(蓝色)的发射偏振角度分别是 114°和 66°;(d)平行和垂直激发偏振下纳米线(红色)的发射偏振角度分别为 −6°和 66°

Fig. 6 Calculated emission polarization of nanowire and triangular plate. (a) Schematic of Ag nanowire-triangular plate “line” coupling; (b) localized electric field distribution; (c) emission polarization angle of triangular plate (blue) is 114° and 66° under parallel and perpendicular excitation polarization, respectively; (d) emission polarization angle of nanowire (red) is −6° and 66° under parallel and perpendicular excitation polarization, respectively

所示，此时纳米线中等离激元模式的发射与激发偏振大致相同，因此，发射偏振会随着激发偏振的旋转而旋转。这种情况可以在实验中观察到，如图 2 所示。然而，当三角片与纳米线之间为“点”接触时，电场主要分布在三角片上。尽管从近场角度无法直接得到偶极子分布，但可以通过计算 J 积分得到不同激发偏振下三角片产生的远场辐射的偏振方向约为 160°。此情况在实验和模拟中均得到了证实，如图 3(c)和图 4(c)所示。

4 结　论

用湿化学合成方法制备了银纳米线-三角片耦合结构，研究了耦合处的发射偏振与入射偏振之间的依赖关系。结果发现：当三角片与纳米线呈“线”接触耦合时，发射光的偏振会随着激发偏振的变化而变化；当三角片与纳米线呈“点”接触时，发射光的偏振角度几乎保持 160°不变。通过建立理论模型以及计算自由电流密度体积分得到：当纳米线与三角片“线”接触时，在间隙处会形成法布里-珀罗腔，此时纳米线中的等离激元模式占主导；当纳米线与三角片“点”接触时，耦合处的发射主要由三角片中的等离激元模式主导。因此，可以通过改变三角片与纳米线的耦合方式来调控耦合体系的发射偏振依赖性。本研究表明可以通过构建耦合的波导结构来实现光偏振态的调控，从而为集成纳米光子器件的发展提供新的技术路线。

参　考　文　献

[1] Ritchie R H. Plasma losses by fast electrons in thin films[J]. Physical Review, 1957, 106(5): 874-881.

[2] Gramotnev D K, Bozhevolnyi S I. Plasmonics beyond the diffraction limit[J]. Nature Photonics, 2010, 4(2): 83-91.

[3] Barnes W L, Dereux A, Ebbesen T W. Surface plasmon subwavelength optics[J]. Nature, 2003, 424(6950): 824-830.

[4] Wu X Q, Xiao Y, Meng C, et al. Hybrid photon-plasmon nanowire lasers[J]. Nano Letters, 2013, 13(11): 5654-5659.

[5] Clark B D, Lou M H, Nordlander P, et al. Aluminum nanocrystals grow into distinct branched aluminum nanowire morphologies[J]. Nano Letters, 2020, 20(9): 6644-6650.

[6] 刘杰，陈炫任，王小云，等. 表面等离激元-光子混合波导中共振能量转移增强[J]. 光学学报，2022，42(15)：1513002.
Liu J, Chen X R, Wang X Y, et al. Enhancement of resonance energy transfer in surface plasmon-photon hybrid waveguide[J]. Acta Optica Sinica, 2022, 42(15): 1513002.

[7] Niu Y J, Xu H X, Wei H. Unified scattering and photoluminescence spectra for strong plasmon-exciton coupling[J]. Physical Review Letters, 2022, 128(16): 167402.

[8] Bozhevolnyi S I, Volkov V S, Devaux E, et al. Channel plasmon subwavelength waveguide components including interferometers and ring resonators[J]. Nature, 2006, 440(7083): 508-511.

[9] Shegai T, Miljković V D, Bao K, et al. Unidirectional broadband light emission from supported plasmonic nanowires[J]. Nano Letters, 2011, 11(2): 706-711.

[10] Yang L K, Li P, Li Z P. Plasmonic polarization beam splitting based on single silver nanowire[J]. Optics Express, 2019, 27(4): 3851-3860.

[11] Dongare P D, Zhao Y G, Renard D, et al. A 3D plasmonic antenna-reactor for nanoscale thermal hotspots and gradients[J]. ACS Nano, 2021, 15(5): 8761-8769.

[12] 靳延平，杨勇，徐新龙. 基于纳米天线阵列非线性光学效应的太赫兹辐射特性研究[J]. 光学学报，2022，42(15)：1506001.
Jin Y P, Yang Y, Xu X L. Terahertz radiation characteristics based on nonlinear optical effect of nano-antenna array[J]. Acta Optica Sinica, 2022, 42(15): 1506001.

[13] Foster M A, Turner A C, Sharping J E, et al. Broad-band optical parametric gain on a silicon photonic chip[J]. Nature, 2006, 441(7096): 960-963.

[14] Koos C, Vorreau P, Vallaitis T, et al. All-optical high-speed signal processing with silicon–organic hybrid slot waveguides[J]. Nature Photonics, 2009, 3(4): 216-219.

[15] Chen H, Jiang Z H, Hu H T, et al. Sub-50-ns ultrafast upconversion luminescence of a rare-earth-doped nanoparticle[J]. Nature Photonics, 2022, 16(9): 651-657.

[16] Lal S, Link S, Halas N J. Nano-optics from sensing to waveguiding[J]. Nature Photonics, 2007, 1(11): 641-648.

[17] Shen S X, Meng L Y, Zhang Y J, et al. Plasmon-enhanced second-harmonic generation nanorulers with ultrahigh sensitivities [J]. Nano Letters, 2015, 15(10): 6716-6721.

[18] Chen W, Zhang S P, Deng Q, et al. Probing of sub-picometer vertical differential resolutions using cavity plasmons[J]. Nature Communications, 2018, 9: 801.

[19] 王琳，张磊. 基于表面等离激元谐振腔的窄谱增强传感器[J]. 光学学报，2021，41(7)：0724001.
Wang L, Zhang L. Narrow-spectrum enhanced sensor based on surface plasmon resonator[J]. Acta Optica Sinica, 2021, 41(7): 0724001.

[20] 曹瑗琛，倪海彬，倪波，等. 自组装银纳米环等离激元生物传感器的制备与光学性质[J]. 中国激光，2022，49(3)：0313001.
Cao A C, Ni H B, Ni B, et al. Preparation and optical properties of self-assembled plasmonic biosensor based on silver nanoring[J]. Chinese Journal of Lasers, 2022, 49(3): 0313001.

[21] Gisin N, Ribordy G, Tittel W, et al. Quantum cryptography[J]. Reviews of Modern Physics, 2002, 74(1): 145-195.

[22] Li Z P, Bao K, Fang Y R, et al. Correlation between incident and emission polarization in nanowire surface plasmon waveguides[J]. Nano Letters, 2010, 10(5): 1831-1835.

[23] Knight M W, Grady N K, Bardhan R, et al. Nanoparticle-mediated coupling of light into a nanowire[J]. Nano Letters, 2007, 7(8): 2346-2350.

[24] Wei H, Hao F, Huang Y Z, et al. Polarization dependence of surface-enhanced Raman scattering in gold nanoparticle-nanowire systems[J]. Nano Letters, 2008, 8(8): 2497-2502.

[25] Fang Y R, Wei H, Hao F, et al. Remote-excitation surface-enhanced Raman scattering using propagating Ag nanowire plasmons[J]. Nano Letters, 2009, 9(5): 2049-2053.

[26] Hutchison J A, Centeno S P, Odaka H, et al. Subdiffraction limited, remote excitation of surface enhanced Raman scattering[J]. Nano Letters, 2009, 9(3): 995-1001.

[27] Camargo P H C, Cobley C M, Rycenga M, et al. Measuring the surface-enhanced Raman scattering enhancement factors of hot spots formed between an individual Ag nanowire and a single Ag nanocube[J]. Nanotechnology, 2009, 20(43): 434020.

[28] Li Y Y, Li P, Zhang M, et al. Correlations between incident and emission polarization in nanowire-particle coupled junctions[J]. Optics Express, 2022, 30(16): 29206-29215.

[29] Fang Y R, Li Z P, Huang Y Z, et al. Branched silver nanowires as controllable plasmon routers[J]. Nano Letters, 2010, 10(5): 1950-1954.

[30] Wei H, Pan D, Xu H X. Routing of surface plasmons in silver nanowire networks controlled by polarization and coating[J]. Nanoscale, 2015, 7(45): 19053-19059.

[31] Yan R X, Pausauskie P, Huang J X, et al. Direct photonic-plasmonic coupling and routing in single nanowires[J]. Proceedings of the National Academy of Sciences of the United States of America, 2009, 106(50): 21045-21050.

[32] Hua J J, Wu F, Xu Z F, et al. Influence of symmetry breaking

degrees on surface plasmon polaritons propagation in branched silver nanowire waveguides[J]. Scientific Reports, 2016, 6: 34418.
[33] Agreda A, Sharma D K, des Francs G C, et al. Modal and wavelength conversions in plasmonic nanowires[J]. Optics Express, 2021, 29(10): 15366-15381.
[34] Li Z P, Zhang S P, Halas N J, et al. Coherent modulation of propagating plasmons in silver-nanowire-based structures[J]. Small, 2011, 7(5): 593-596.
[35] Dicken M J, Sweatlock L A, Pacifici D, et al. Electrooptic modulation in thin film barium titanate plasmonic interferometers [J]. Nano Letters, 2008, 8(11): 4048-4052.
[36] Dionne J A, Diest K, Sweatlock L A, et al. PlasMOStor: a metal-oxide-Si field effect plasmonic modulator[J]. Nano Letters, 2009, 9 (2): 897-902.
[37] Pan D, Wei H, Xu H X. Optical interferometric logic gates based on metal slot waveguide network realizing whole fundamental logic operations[J]. Optics Express, 2013, 21(8): 9556-9562.
[38] Wei H, Li Z P, Tian X R, et al. Quantum dot-based local field imaging reveals plasmon-based interferometric logic in silver nanowire networks[J]. Nano Letters, 2011, 11(2): 471-475.
[39] Wei H, Wang Z X, Tian X R, et al. Cascaded logic gates in nanophotonic plasmon networks[J]. Nature Communications, 2011, 2: 387.
[40] Li Z P, Hao F, Huang Y Z, et al. Directional light emission from propagating surface plasmons of silver nanowires[J]. Nano Letters, 2009, 9(12): 4383-4386.
[41] Zhang S P, Wei H, Bao K, et al. Chiral surface plasmon polaritons on metallic nanowires[J]. Physical Review Letters, 2011, 107(9): 096801.
[42] Jackson J D, Levitt L C. Classical electrodynamics[J]. Physics Today, 1962, 15(11): 62.

Polarization Dependence Between Excitation and Emission in Nanowire-Triangular Plate Coupled Structures

Li Yuanyuan, Yang Longkun, Li Zhipeng*

Beijing Key Laboratory of Nano-Photonics and Nano-Structure (NPNS), Department of Physics, Capital Normal University, Beijing 100048, *China*

Abstract

Objective Surface plasmon polaritons (SPPs) supported by metallic nanostructures can confine electromagnetic fields at the nanoscale and overcome the diffraction limit. Compared with conventional electronic devices, integrated subwavelength optical devices with high data transmission rates and wide bandwidths provide a promising platform for the development of nanophotonics. In recent decades, various plasmon-based optical elements have been developed, including waveguides, resonators, nanoantennas, multiplexers, and switchers. Polarization-controllable optical elements are important in chip-to-chip interconnects, sensors, and quantum cryptography. Chemically synthesized nanowires have been reported to function as polarization-controllable plasmonic waveguides, where the emission of different SPPs modes relies on the shape of the wire end. Additionally, optical properties sensitive to incident polarization have been observed in coupled nanostructures composed of wires or nanoparticles. For example, the near-field enhancement and far-field emission polarization of coupled junctions can be modulated via incident polarization, through which polarization-dependent routers, modulators, and logic gates have been achieved. Hence, further optimization of coupled waveguides can provide additional flexibility for controlling light polarization at the nanoscale. In this study, we investigated the correlations between the emission and incident polarization of a nanowire-triangular plate coupled structure. The results indicate that the polarization dependence can be modulated by the wire-triangular plate coupling type. The response of the emission polarization to the incident polarization is verified using the finite-difference time-domain (FDTD) method. In theory, by calculating the volume integration of the free current density, the conversion of propagating SPP modes and wire-triangular plate coupled mode can be revealed. The emission mechanism of the coupled structures can be elucidated based on the superposition of different SPP modes. The findings provide a new degree of freedom for manipulating light polarization at the nanoscale, and are beneficial to the development of plasmonic nanophotonics.

Methods In this study, we fabricated silver nanowire-triangular plate coupled structures using a typical chemical method. A dilute ethanol suspension comprising nanowires and triangular plates was drop-cast onto an indium tin oxide-coated glass slide, where the coupled structures were self-assembled after drying under ambient conditions. Scanning electron microscopy was used to distinguish the different coupled structures, as shown in Figs. 2(a) and 3(a). Subsequently, the samples were immersed promptly in an index-matched oil with $n=1.518$ to protect the samples against oxidization or sulfuration in air. Next, optical measurements were performed, where He-Ne laser with a wavelength of 633 nm was focused onto the nanowire end through an oil objective. The response of the emission polarization to the incident polarization was obtained by rotating the half-wave plate and polarizer. The experimental data were verified via simulation using the FDTD method, and the emission mechanism was determined by calculating the volume integration of the free current density.

Results and Discussion The experimental results show different polarization correlations between the excitation and emission of the nanowire-triangular plate coupled structure. The emission polarization follows the direction of the excitation polarization. Meanwhile, the emission polarization is maintained at 160°, regardless of the incident polarization. In the simulation, we recorded the

local near-field distribution and obtained the corresponding far-field emission using the FDTD method. When the triangular plate-nanowire coupling exhibits a "line" connection, the emission polarization increases monotonically with the incident polarization. However, when the coupling type exhibits a "point" connection, the emission polarization remains at 160°, regardless of the incident light. These experimental and simulation results show that the emission behaviors can be effectively modulated by the wire-triangular plate coupling type. To elucidate the modulation mechanism, we analyzed the plasmon modes excited in the nanowire-triangular plate junction. The three modes contribute to the emission from the junction: hybridized wire modes $m=0$ and $m=1$ and the nanowire-triangular plate coupling mode P (Fig. 5). Based on antenna radiation theory and the volume integration of the free current density, we calculate the emission contributed by the triangular plate and nanowire. The results show that the light emitted from the triangular plate is always polarized at 160°, regardless of the incident polarization. It can be understood by the fact that the orientation of induced dipole oscillation is 160°. In addition, the emission polarization from the wire part is the same as the incident polarization. Hence, when the triangular plate-nanowire exhibits "wire" coupling, the junction serves as a Fabry-Perot cavity and the wire modes dominate the emission polarization rotating with the incident polarization. When the triangular plate-nanowire exhibits a "point" connection, the near-field is mainly localized on the triangular plate, in which the emitted light dominated by coupling mode P with polarization remains in the 160° orientation.

Conclusions We fabricated silver nanowire-triangular plate coupled structures via wet chemical synthesis and investigated their polarization correlations between incident light and emission. The results showed that the incidence-emission polarization correlation depended on the coupling type of the nanowire-triangular plate. When the triangular plate-nanowire exhibited a "line" connection, a Fabry-Perot cavity was formed in the junction. The polarization of the emitted light followed with the excitation polarization. However, for the "point" coupling type, the emission polarization remained at 160°, regardless of the incident polarization. The emission mechanism can be interpreted by the superposition of propagating SPP modes and the localized mode of the coupled nanowire-triangular plate structure. Hence, the emission polarization at the junction can be manipulated by the nanowire-triangular plate coupling type. These findings can be used to develop more sophisticated polarization-controllable devices and are beneficial to the development of integrated nanophotonics.

Key words optical materials; surface plasmon polaritons; nanostructures; emission; polarization dependence